batteries

MDPI

Article

Validity of LiPON Conductivity Determined by Impedance Spectroscopy

Alexander Rudy [1,*], Alena Novozhilova [2] and Julia Egorova [1]

[1] Laboratory of Physics and Electrochemistry of Solid-State Current Sources, Scientific Research Department, P.G. Demidov Yaroslavl State University, Yaroslavl 150003, Russia; tortseva.julia@mail.ru
[2] Research Laboratory of Materials and Components of Conventional Energy, Complex of Innovations and Technologies, RUDN University, Moscow 117198, Russia; alena.novozhilova.2014@mail.ru
* Correspondence: rudy@uniyar.ac.ru

Abstract: A hypothesis that the generally accepted value of the LiPON conductivity should be attributed to the absorption and displacement currents is substantiated. The reason is a small contribution of the drift current due to field screening by the electric double layer. The basis for this assumption is the measurement of the LiPON absorption capacitance, according to which its dielectric constant is about 10^6. An alternative equivalent circuit containing a non-ideal absorption element is proposed and its impedance is calculated. It is shown that the Bode diagrams of the alternative circuit approximate the experimental curves well. Parameters and the magnitude of electric field screening are calculated based on a proposed model of a double electric layer. Considering the screening effect, the drift conductivity of LiPON is obtained, which is in good agreement with the data on lithium concentration and ion mobility.

Keywords: solid electrolyte; impedance spectroscopy; absorption current; electric double layer; Debye length; drift conductivity

check for updates

Citation: Rudy, A.; Novozhilova, A.; Egorova, J. Validity of LiPON Conductivity Determined by Impedance Spectroscopy. *Batteries* **2024**, *10*, 245. https://doi.org/10.3390/batteries10070245

Academic Editor: Wilhelm Pfleging

Received: 21 April 2024
Revised: 3 July 2024
Accepted: 5 July 2024
Published: 9 July 2024

1. Introduction

Solid-state thin-film lithium-ion batteries (SSLIB) are a relatively new and promising type of chemical energy storage device. It is no exaggeration to say that the performance characteristics of SSLIBs are determined primarily by the conductivity of the solid electrolyte. In recent years, significant progress has been made in the development of new inorganic electrolytes. Here, first, it should be noted that glassy sulfides [1–9], of which the most popular are $Li_{10}GeP_2S_{12}$ (LGPS) and Li_6PS_5X (LPS), where X = Cl, Br, and I, demonstrate very high ionic conductivity of $1.9{\cdot}10^{-3}$ S·cm^{-1} and $6.8{\cdot}10^{-3}$ S·cm^{-1}. Crystalline electrolytes have lower conductivity but greater resistance to water and atmospheric gases [10–22], and the most promising materials are considered to be crystalline solid electrolytes with NASICON structure. Of the NASICON-like electrolytes, the most in demand is the Li^+-conducting electrolyte $Li_{1.3}Al_{0.3}Ti_{1.7}(PO_4)_3$ (LATP), which belongs to the family with the general formula (M = Al, Ga, In, Sc). In [23], a LATP exhibiting ionic conductivity $1.4{\cdot}10^{-4}$ S·cm^{-1} and activation energy for Li diffusion of 0.253 eV was reported.

Among the glassy electrolytes, the most popular is lithium phosphorus oxynitride (LiPON), developed in the mid-1990s by J. Bates et al. at Oak Ridge National Laboratory. The conductivity of LiPON is $\sigma = 2{\cdot}10^{-6}$ S·cm^{-1} [24], which is significantly lower than that of LATP. But due to its high manufacturability, wide potential window, and low electron transference number, LiPON is used in the vast majority of industrial thin-film batteries. Therefore, the mechanisms of charge transfer in LiPON and methods for studying them are still relevant. The most important LiPON characteristics were reported by J. Bates et al. in [24–30]. Later, these results were confirmed in subsequent works by J. Bates et al., as well as experimental [31–38] and theoretical [39] studies by other authors. In all cases, conductivity was understood as drift conductivity, which characterizes the ability of the

electrolyte to transport lithium ions. It is shown below that, for a number of reasons, the experimentally obtained conductivity values must be attributed to the absorption current.

2. Generally Accepted LiPON Equivalent Circuits and Their Validity

As a sample for measuring the conductivity of LiPON via impedance spectroscopy, an electrolyte film ~1 μm thick with metallization strips deposited on its opposite surfaces is used. To reduce parasitic capacitance, the strips are deposited crosswise, and their width usually does not exceed several millimeters. Typical results of impedance spectroscopy of such samples in the form of Nyquist diagrams can be found in [31–38]. Despite the visual homothety of Nyquist diagrams, LiPON equivalent circuits show some diversity, but almost all of them contain the standard set of obligatory structural elements (Z_i, Z_{el}, R_{el}) shown in Figure 1. The elements Z_i and Z_{el} are constant phase elements (CPE) $\hat{Z} = A(j\omega)^{-\alpha}$, where A is a physical quantity of dimension $\Omega \cdot s^{1-\alpha}$, α is the non-ideality factor, ω is the cyclic frequency, and j is the imaginary unit. As a rule, for Z_i, the non-ideality factor is a value close to unity; therefore, it is usually interpreted as a capacitor with a leakage. Although the leakage current is an experimental fact, the imperfection of the capacitor may be also due to the dielectric with high ionic relaxation permittivity. The Z_{el} nonideality factor is about 0.5, which allows for Z_{el} interpretation as a nonideal diffusion element. Taken together, all three elements (Z_i, Z_{el}, R_{el}) have resistance to the displacement current, although this is not stated directly anywhere.

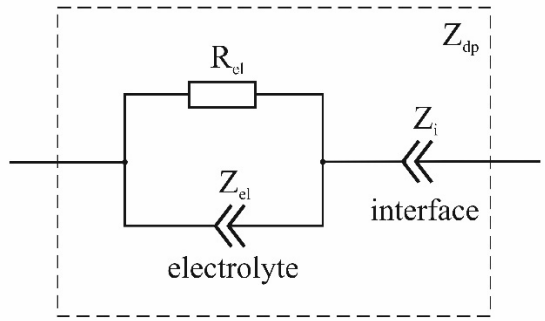

Figure 1. The core part of the conventional equivalent circuits of the M | LiPON | M sandwich structure.

Since the charge carriers in LiPON are lithium ions, while in the rest of the circuit the charge is transported by electrons, the current through LiPON cannot be a conduction current. The exception is the through-current caused by Faraday processes at the boundary. But due to its smallness, this current can be neglected. The generally accepted equivalent circuits (Figure 1) do not contradict this statement, since they contain capacity Z_i, which breaks the conduction current circuit. However, the dissipative elements Z_{el} and R_{el} in series with capacity do not reflect the real resistance mechanism because this implies that the current in the LiPON volume consists only of drift and diffusion components. LiPON, as will be shown below, has a very high dielectric constant; therefore, the electric field in the bulk and the drift current are minor. The electric field does not affect the diffusion current, but due to the small size of the lithium diffusion coefficient, it is of the same order as the absorption current or even less. Therefore, drift currents cannot provide the experimentally observed conductivity, which means that the main contribution to conductivity comes from the absorption and diffusion currents.

Displacement currents are a fairly broad concept and include the displacement current itself $I_{dp} = Sd(\varepsilon_0 E(t))/dt$, the absorption current $I_A = Sd(\varepsilon_0 \varepsilon(\omega) E(t))/dt$, and $I_{dp} + I_A$. Where S is the sample area, ε_0 is the electric constant, $\varepsilon(\omega)$ is the dielectric constant of LiPON, and $E(t)$ is the alternating electric field strength. From the second expression, it is clear that, with the dielectric constant of the electrolyte $\varepsilon(\omega) \gg 1$, the absorption current can exceed the displacement current by orders of magnitude. To avoid confusion below, the term displacement current is used for the total current through the sample, and the term

absorption current is used only for the current due to the polarization of the electrolyte. In symbolic form, the total current is $I_{dp} = I_A + I_R + I_W$, where I_R and I_W are the drift and diffusion currents. Thus, to consider dielectric losses (polarization losses), it is necessary to add to the conventional equivalent circuit an absorption element in parallel with the diffusion element and active resistance.

It must be also kept in mind that the active resistance obtained as a result of parameter fitting does not reflect the real resistance to the drift current, because the electric field strength in the volume is weakened by a factor of $\varepsilon(\omega)$. As a result of experimental curve approximation, one obtains a certain apparent resistance R, which is related to the intrinsic resistance R_{int} by the expression $R = \varepsilon(\omega)R_{int}$. Since active resistance does not depend on frequency, this relationship can be represented as $R = \varepsilon(0)R_{int}$. Therefore, the active resistance R in a conventional equivalent circuit must be treated as an apparent resistance $R = \varepsilon(0)R_{int}$.

The dielectric constant $\varepsilon(0)$ required for the R_{int} calculation can be determined by direct measurements of the M | LiPON | M chemical capacity, as was carried out in [40]. The capacity of a Pt | LiPON | Pt sandwich structure with an area of $S = 0.64$ cm^2 and a thickness of $d = 1$ μm was measured using the circuit displayed in Figure 2a. The voltage across the structure versus time is shown in Figure 2b. The LiPON chemical capacity was calculated as

$$Q = \frac{U_0}{R_0}T - \left(\frac{1}{R_0} + \frac{1}{R_{pt}}\right)A(T) \quad (1)$$

where T is the saturation time and $A(T) = \int_0^T U_c(t)dt$ is the area under the curve in Figure 2b. For $T = 550$ s, Equation (1) gives $Q = 9.26 \cdot 10^{-4}$ C, which allows us to find the capacitance $C = Q/U_c(T) = 9.08 \cdot 10^{-4}$ F. On the other hand, the capacitance of a parallel-plate capacitor is $C = \varepsilon_0\varepsilon(0)S/d$, which lets us find the dielectric constant $\varepsilon(0) = 1.6 \cdot 10^6$ and dielectric susceptibility $\chi \approx 1.6 \cdot 10^6$. For comparison, the dielectric constant of borosilicate or phosphate glass is on the order of several units, and the maximum dielectric constant of ferroelectrics barely reaches 10^5 [41]. The current that is maintained for 550 s in the galvanically unconnected circuit cannot be anything other than an absorption current of mobile lithium ions. This is confirmed by two other plots in Figure 2b, recorded at temperatures of −26 °C and −50 °C. At low temperatures, in accordance with the Arrhenius law, the concentration of mobile lithium ions decreases, as does the lifetime of the absorption current. For the same reason, the dielectric constant of LiPON decreases.

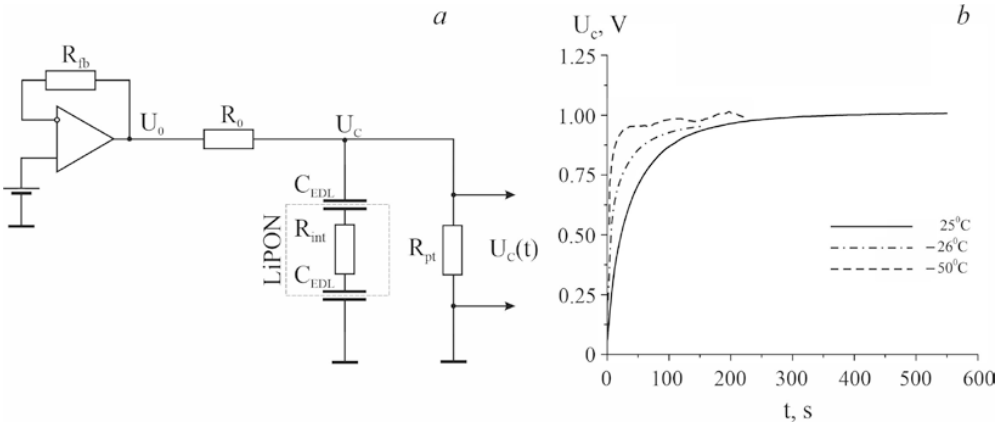

Figure 2. (**a**) Scheme for measuring the absorption current and chemical capacity of the Pt | LiPON | Pt structure, where $U_0 = 1.18$ V, $R_0 = 100$ kΩ, and $R_{pt} = 1$ MΩ. (**b**) Time dependence of voltage across the Pt | LiPON | Pt structure [40].

3. Alternative Equivalent Circuit of LiPON

Figure 2 depicts the alternative equivalent circuit of the M | LiPON | M sandwich structure that considers the absorption current and the electric field screening by the electric double layer (EDL). Absorption element A determines the absorption current; element W_1 simulates the resistance to the diffusion current; the capacitor C_{EDL} models the EDL capacitance; and the resistor R simulates the apparent resistance, which is related to the intrinsic ohmic resistance as $R = \varepsilon(0)R_{int}$. The last two elements, W_2 and R_{lk}, form the leakage circuit. The resistor R_{lk} limits the rate of the Faraday process at the cathode, while the Warburg element W_2 determines the diffusion rate of reduced lithium atoms to the anode. The leakage current circuit is necessary for correct impedance spectra approximation in the low-frequency region, where the conductivity of capacitor C_{EDL} tends to be zero. In Figure 2, W_1 and W_2 are semi-infinite Warburg diffusion elements, the impedance of which is further designated as $Z_{W1,2} = Z'_{W1,2} + j\,Z''_{W1,2}$, where $Z'_{W1,2} = A_{W1,2}/\sqrt{\omega}$, $Z''_{W1,2} = -A_{W1,2}/\sqrt{\omega}$, and $A_W = U_0/\sqrt{2D}Sqc_0$ is the Warburg coefficient.

In accordance with the conventional algorithm, to strictly derive an absorption element impedance, it is necessary to consider the boundary value problem on the electromagnetic wave propagation. Considering the heterogeneity of the medium in which electric induction $\vec{D}(x)$ is a function of the coordinate, such a problem seems difficult to solve. Therefore, the absorption element is considered as a system with lumped parameters for which the problem of medium inhomogeneity automatically vanishes. The absorption current is obtained as a derivative of the electric induction.

$$I_A = S\frac{dD}{dt} = j\omega S\varepsilon_0\varepsilon_{el}(\omega)E_0e^{j\omega t} \tag{2}$$

where $E_0 = U_0/d$, U_0 is the applied voltage amplitude, d is the LiPON thickness, S is the electrode area, ω is the cyclic frequency, ε_{el} is the dielectric constant of the electrolyte, and j is an imaginary unit. The impedance is found as the ratio of voltage to absorption current:

$$Z_A = \frac{d}{j\omega S\varepsilon_0\varepsilon_{el}(\omega)} \tag{3}$$

To approximate the dielectric constant, the Cole and Cole model is used:

$$\varepsilon_{el}(\omega) = \frac{\varepsilon_{el}(0) - \varepsilon_\infty}{1 + (j\omega\tau)^\beta} + \varepsilon_\infty \tag{4}$$

as appropriate for both resonant and relaxation oscillations [42], where τ is the relaxation time. The nonideality factor β is related to the corresponding parameter of the Cole and Cole equation as $\beta = 1 - \alpha$. Substituting (3) into (2) allows us to find the real and imaginary parts of the impedance Z_A:

$$\begin{aligned} Z'_A &= \frac{A_A}{\omega}\frac{(1-\rho)(\omega\tau)^\beta \sin\left(\beta\frac{\pi}{2}\right)}{1+2\rho(\omega\tau)^\beta\cos\left(\beta\frac{\pi}{2}\right)+\rho^2(\omega\tau)^{2\beta}}, \\ Z''_A &= -\frac{A_A}{\omega}\frac{1+\rho(\omega\tau)^{2\beta}+(1+\rho)(\omega\tau)^\beta\cos\left(\beta\frac{\pi}{2}\right)}{1+2\rho(\omega\tau)^\beta\cos\left(\beta\frac{\pi}{2}\right)+\rho^2(\omega\tau)^{2\beta}}, \end{aligned} \tag{5}$$

where $\rho = \varepsilon_\infty/\varepsilon_{el}(0)$, $A_A = d/S\varepsilon_0\varepsilon_{el}(0)$.

The total impedance $Z = Z' + jZ''$ of the circuit in Figure 3 is as follows:

$$\begin{aligned} Z' &= R\frac{RZ'_{AW}+|Z_{AW}|^2}{(R+Z'_{AW})^2+Z''^2_{AW}} + \left(\frac{2}{\omega C_{EDL}}\right)^2\frac{R_{lk}+\frac{A_{W2}}{\sqrt{\omega}}}{\left(R_{lk}+\frac{A_{W2}}{\sqrt{\omega}}\right)^2+\left(\frac{A_{W2}}{\sqrt{\omega}}+\frac{2}{\omega C_{EDL}}\right)^2}, \\ Z'' &= \frac{R^2Z''_{AW}}{(R+Z'_{AW})^2+Z''^2_{AW}} - \frac{2}{\omega C_{EDL}}\frac{\frac{A_{W2}}{\sqrt{\omega}}\left(\frac{A_{W2}}{\sqrt{\omega}}+\frac{2}{\omega C_{EDL}}\right)+\left(R_{lk}+\frac{A_{W2}}{\sqrt{\omega}}\right)^2}{\left(R_{lk}+\frac{A_{W2}}{\sqrt{\omega}}\right)^2+\left(\frac{A_{W2}}{\sqrt{\omega}}+\frac{2}{\omega C_{EDL}}\right)^2}, \end{aligned} \tag{6}$$

where

$$Z'_{AW} = \frac{|Z_A|^2 Z'_{W1} + |Z_{W1}|^2 Z'_A}{(Z'_{dp}+Z'_{W1})^2+(Z''_{dp}+Z''_{W1})^2},$$
$$Z''_{AW} = j\frac{|Z_A|^2 Z''_{W1} + |Z_{W1}|^2 Z''_A}{(Z'_A+Z'_{W1})^2+(Z''_A+Z''_{W1})^2} \quad (7)$$

are the real and imaginary parts of the impedance of W_1 and A parallel connection, where

$$|Z_A|^2 = Z'^2_A + Z''^2_A, \ |Z_{W1,2}|^2 = 2\frac{A^2_{W1,2}}{\omega} \quad (8)$$

are module squares of absorption and Warburg impedances.

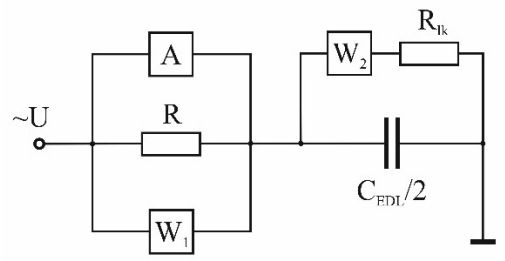

Figure 3. Alternative equivalent circuit where element A models the absorption and displacement current, elements R and W_1 determine drift and diffusion charge transfer, $C_{EDL}/2$ models two EDL in series, and elements W_2 and R_{lk} form the leakage current circuit.

Bode plots of Pt | LiPON | Pt impedance spectrum are shown in Figure 4a. The parameters of the approximating Expressions (4)–(7) are given in the caption to the figure. The parameters R_{lk} and A_{w2} cannot be determined by fitting because they affect only the low-frequency part of the impedance spectrum, which is absent in an appropriate plot [28]. Figure 4a depicts the plots identical to experimental Bode diagrams by J. Bates et al. in black. Colored curves are the plots approximating Expressions (5)–(8). Panel b in Figure 4 depicts the amplitudes of absorption and diffusion currents. As follows from the figure, the absorption current always exceeds the diffusion current. Since the drift current is orders of magnitude smaller than the other two currents, it is omitted from Figure 4b.

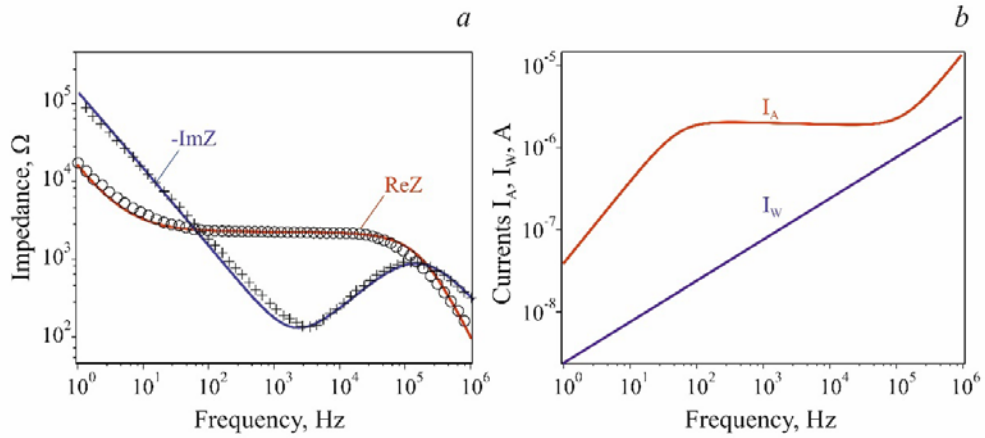

Figure 4. (**a**) Real and imaginary parts of the LiPON impedance. The patterns in black depict the plots identical to Bode diagrams by J. Bates et al. [28]. The colored curves are the plots of the approximating Equations (5)–(8) at parameter values of $\tau = 0.017$ s; $\beta = 1.015$; $C_{EDL} = 9.7{\cdot}10^{-5}$ F; $R = 5{\cdot}10^8$ Ω; $\rho = 3.5{\cdot}10^{-4}$; $A_{W1} = 1.5{\cdot}10^6$ Ω·s$^{-1/2}$; and $A_A = 1.31{\cdot}10^5$ Ω·s^{-1}. R_{lk} and A_{W2} are not defined. (**b**) Amplitudes of absorption I_A current and diffusion current I_W at $U_0 = 5{\cdot}10^{-3}$ V. The amplitude of the drift current $I_{dr} = 10^{-11}$ A is not shown in the figure.

Typically, the results of impedance spectroscopy are presented in the form of Nyquist diagrams [31–38], which provide greater clarity than Bode diagrams. For the convenience of comparing with the results of other authors, the LiPON impedance is depicted in Figure 5 as a Nyquist diagram, generated using the fitting parameters given in the caption to Figure 3. The plots in Figure 5 and Nyquist diagrams from [31–38] are visually homothetic and can be converted to each other by some adjustments to the fitting parameters. In some of the mentioned works, the conjugation of the circle with the low-frequency branch of the spectrum appears to be smoother. Within the framework of the model described by Equation (6), this part of the spectrum depends on the parameter β, which in our case is greater than unity. The view of the Nyquist diagram at $\beta < 1$ is shown in Figure 5 by the dashed line. This is the only dimensionless parameter and, therefore, the one with no physical meaning. As for the rest, the alternative equivalent circuit (Figure 3) contains only ideal elements, which allows us to obtain the kinetic coefficients and electrical parameters of the simulated system.

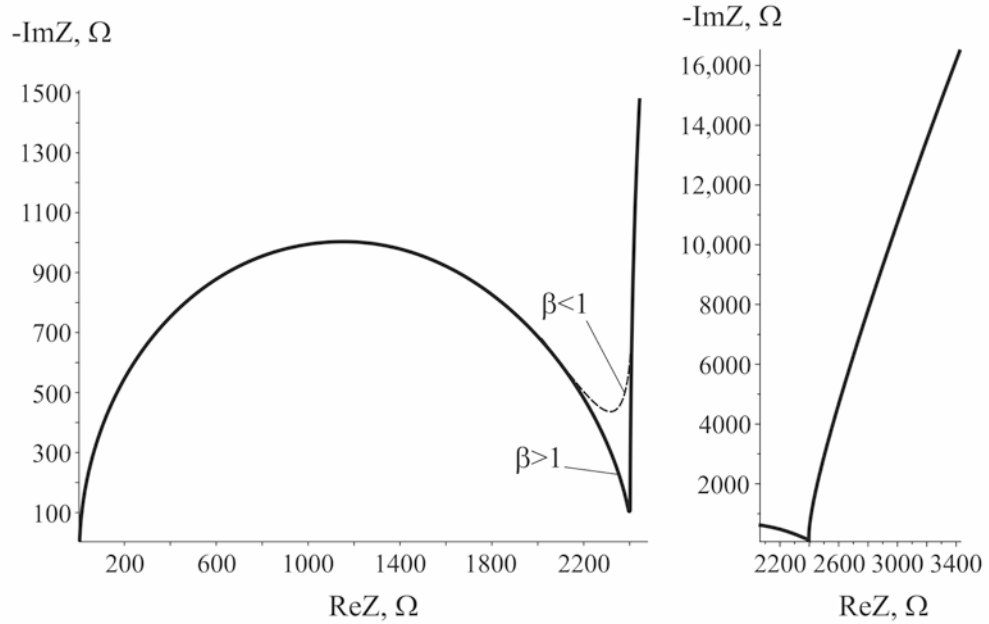

Figure 5. LiPON impedance spectrum in the form of a Nyquist diagram for the same parameter values as in Figure 3. The view of the Nyquist diagram at $\beta < 1$ is shown by the dashed line.

To verify the adequacy of the proposed model, the fitting parameters can be compared with that of [28] and the results of direct measurements [40] (Table 1). Since, in Figure 2b, the ideal element $C_{EDL}/2$ models the capacitance of the entire Pt | LiPON | Pt sandwich structure, the relation $C_{EDL}/2 = \varepsilon_0\varepsilon(0)S/d$ is valid, which allows us to find the dielectric constant $\varepsilon(0) = C_{EDL}d/2S\varepsilon_0$. For $S = 4{\cdot}10^{-6}$ m^2 and $d = 10^{-6}$ m, this relation gives $\varepsilon(0) = 1.37{\cdot}10^6$, which is very close to the result of direct measurements (Table 1). According to the relation $R_{int} = R/\varepsilon(0)$ the intrinsic resistance of LiPON is $R_{int} = 3.65{\cdot}10^2$ Ω and the corresponding conductivity value is $\sigma_{int} = 6.85{\cdot}10^{-6}$ S·cm^{-1}. This conductivity can only be compared with theoretical results or with calculations based on the lithium ion concentration and mobility data. For the diffusion coefficient $D = 1.5{\cdot}10^{-11}$ cm^2·s^{-1} [43] and the concentration $c = 7.5{\cdot}10^{22}$ cm^{-3} obtained in [39] for the relation Li/P = 3.0, the conductivity is $\sigma_{int} = 7.0{\cdot}10^{-6}$ S·cm^{-1}, which is quite close to the conductivity obtained above (Table 1).

Table 1. Fitting parameters of the equivalent circuit in Figure 2b in comparison with [5,17] data.

S, m^2	d, m	C_{EDL}, μF	ε(0)	$\varepsilon_{el}(0)$	R, Ω	σ_{int}, S/cm	Reference
4×10^{-6}	10^{-6}	97	1.37×10^{6}	2.0×10^{3}	365	6.85×10^{-6}	Present work
4×10^{-6}	10^{-6}	0.77	-	-	231.3	2.3×10^{-6}	[28]
6.4×10^{-5}	10^{-6}	908	1.6×10^{6}	-	-	-	[40]

The real part of the impedance of the absorption element ReZ_A (Figure 4b), which is responsible for dielectric losses, remains almost constant ($ReZ_A = 2.1 - 2.6$ kΩ) over a wide frequency range from ten Hz to one hundred kHz. The corresponding conductivity $\sim 1/ReZ_A$ belongs to the range of values of $1.19 \cdot 10^{-6} - 9.6 \cdot 10^{-7}$ S·cm^{-1}. As one can see, dielectric losses are not much different from ohmic losses, and if there is no orientational polarization or it can be neglected, then there is no fundamental difference between these mechanisms. Both are due to the dissipation of energy and momentum of free lithium ions. The only difference is that within the model, ohmic losses are constant, determined at $\omega \to 0$, while dielectric losses are frequency-dependent. In addition, dielectric losses include energy and momentum dissipation by localized lithium ions, so in the low-frequency limit, they do not turn into ohmic losses. Energy dissipation by bonded ions is probably one of the reasons why the resistance ReZ_A is higher than R_{int}.

Figure 6a depicts the Nyquist diagram in the region of infra-low frequencies (10^{-6}–10^{-2} Hz). Figure 6b shows that with frequency decrease, starting from $\omega = 2 \cdot 10^{-5}$ s^{-1}, in the circuit predominates the drift current. This means that the shape of the curve in Figure 6a is determined by the absorption element A and the Warburg element W_1. The unlimited increase in impedance with decreasing frequency is due to the fact that in this range, the C_{EDL} can be considered as the circuit disconnection; therefore the current in the circuit is determined by W_2. This is indicated by the slope $\pi/4$ of the linear segment of the curve in Figure 6a. These results should be considered as estimates, since in this frequency range, the semi-infinite Warburg elements W_1 and W_2 must be replaced by finite elements.

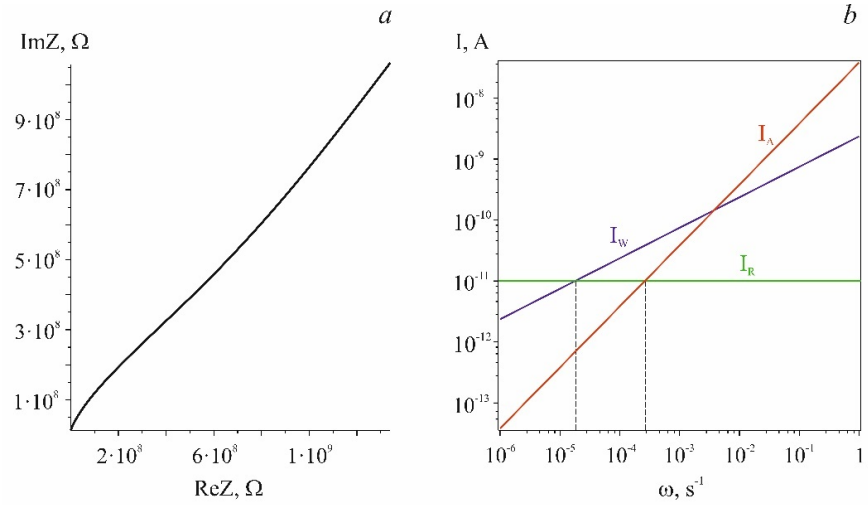

Figure 6. (**a**) Nyquist diagram of Equations (6)–(8) in the infra-low frequency range (10^{-6}–10^{-2} Hz). Parameters of Equations (6)–(8) are indicated in the caption to Figure 4. (**b**) Graphs of absorption (red line), diffusion (blue line), and drift current (green line) currents versus cyclic frequency.

The infra-low frequency range (Figure 6) is of the greatest interest as it complies with SSLIB operating conditions. However, when simulating SSLIB via (6)–(8), the following parameters must be changed. The EDL capacitance should be replaced with the capacitance of the anode–LiPON and cathode–LiPON interfaces connected in series. Resistance R must be reduced in proportion to the capacitance of the series-connected interfaces, the elements

of the leakage circuit must be replaced with the resistance of the interfaces, and semi-finite Warburg elements must be replaced with finite ones.

4. Electric Double Layer

Equations (5)–(8) allow us to generate any Bode or Nyquist diagrams from those given in [28,31–38], but with different fitting parameters. First of all, this applies to the element Z_i, and capacitance increases by two orders of magnitude (Table 1) compared to [28]. In the cited works, the nature of the capacity Z_i is uncertain. In the proposed equivalent circuit, this capacity models a double electrical layer to which the capacitance of the entire Pt | LiPON | Pt sandwich structure is assigned. There are several reasons why this capacity can be considered as EDL. Firstly, in all equivalent circuits, this is an ideal or almost ideal capacity. Secondly, this is the ideal capacity of a large capacitance; therefore, the gap between the plates of the parallel-plate capacitor C_{EDL} must be on an atomic scale. Third, there is experimental evidence of lithium penetration across the metal-LiPON interface, which leads to EDL formation [34,44].

The very hypothesis of EDL is based on the fact that lithium comes out to the surface through any metal electrodes, including platinum. These facts include the products of lithium interaction with the atmosphere in the form of "prominences" [44] or "flower-like features" [34] formed on the surface. The starting point for constructing EDL model is the assumption that the transition of lithium ions into metal occurs as a result of diffusion and is accompanied by their reduction with the formation of a depletion layer. The excess ions of the down-conductor M^+, localized on the surface and cation vacancies O^- (Figure 7) bound by Coulomb forces, form an EDL. It is possible that such a reduction does not occur, but a weakly bound pair $Li^+ - e$ is formed, which, diffusing into the bulk of the metal, reduces the electron density in the interface region. In this case, the depletion layer of the metal will still be localized at the interface due to the Coulomb interaction with cation vacancies. Within an EDL, metal ions act as potential-determining ions, and cation vacancies act as counterions. The configuration of the layer of immobile cation vacancies is determined by the diffusion and drift of lithium ions; therefore, the concept of a "diffuse layer" is applicable to this model. In essence, the EDL is a space charge or depletion layer, but in the present context, considering it as a double electric layer is more appropriate.

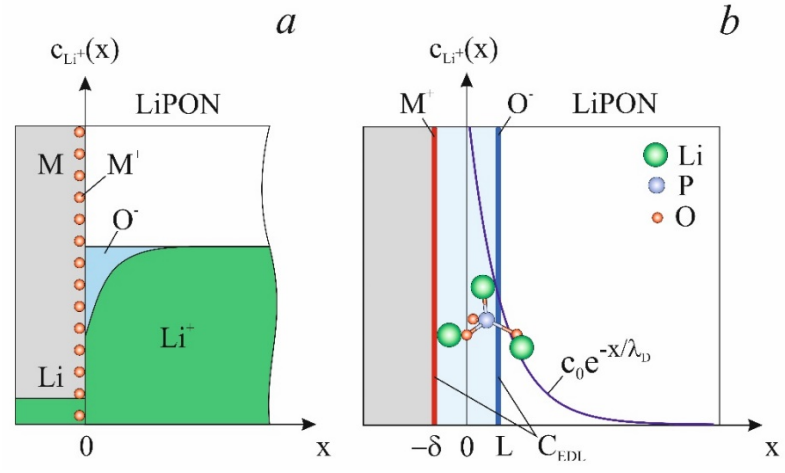

Figure 7. Model of the electrical double layer at the LiPON–metal interface. (**a**) M^+ are potential-determining metal ions; O^- are cation vacancies (counterions). In blue, the diffuse layer formed by uncompensated cation vacancies (depletion layer) is shown. (**b**) EDL simulation by plane capacitor, formed by the metal ion layer and an imaginary plane $x = L$ passing through the center of mass of the counterions. The blue curve depicts the distribution of lithium concentration in the EDL region. The origin of the coordinates is located at a distance $\delta = \ell + r_{Li}$ from the plane of the current collector, where ℓ is the length of the bond $Li^+ - O^-$ and r_{Li} is the radius of the lithium ion. $c_0 = c(0)$ is the maximum concentration of cationic vacancies.

The assumption that the metal ions are potential-determining enables the calculation of the cation vacancies concentration $c(x)$. Typically, the Poisson–Boltzmann equation is used for such calculations, and is applied to systems with a non-conserved number of particles. In this case, the number of cation vacancies is strictly equal to the number of potential-determining ions, and the consideration can be limited by the Poisson equation. Since the concentration distribution in the EDL $c(x)$ is of greatest interest, the solution to the Poisson equation can be obtained last. The concentration can be calculated based on the obvious relation:

$$E(x) = \frac{\rho_{pd}}{\varepsilon_0 \varepsilon} - \frac{q}{\varepsilon_0 \varepsilon} \int_0^x c(x)dx \tag{9}$$

where ρ_{pd} is the surface density of potential-determining ions, q is the elementary charge, and $c(x)$ is the concentration of cation vacancies. The field strength can be expressed from the equilibrium condition for diffusion and drift currents:

$$\sigma E(x) = -qD\frac{dc(x)}{dx} \tag{10}$$

where σ is the ionic conductivity of LiPON and D is the lithium diffusion coefficient. Note that here, the immobile cation vacancies are assigned to the drift and diffusion mobility of lithium ions. Substituting (10) into (9) gives an integral–differential equation, which takes the form of a diffusion equation after differentiation:

$$\frac{d^2}{dx^2}c(x) - \frac{\sigma}{\varepsilon_0 \varepsilon D}c(x) = 0 \tag{11}$$

Solving Equation (11) and satisfying the condition $q\int_0^\infty c(x)dx = \rho_{pd}$ yields the concentration of cation vacancies, field strength, and potential distribution in the EDL:

$$c(x) = \frac{\rho_{pd}}{q}\frac{1}{\lambda_D}e^{-\frac{x}{\lambda_D}} \tag{12}$$

$$E(x) = \frac{\rho_{pd}}{\varepsilon_0 \varepsilon}e^{-\frac{x}{\lambda_D}} \tag{13}$$

$$\left.\begin{array}{l} \varphi(x) = \frac{\rho_{pd}}{\varepsilon_0 \varepsilon}\lambda_D e^{-\frac{x}{\lambda_D}},\ x \in [0, d-\delta] \\ \varphi(x) = \frac{\rho_{pd}}{\varepsilon_0 \varepsilon}(\lambda_D - x),\ x \in [-\delta, 0] \end{array}\right\} \tag{14}$$

where $\lambda_D = \sqrt{\varepsilon_0 \varepsilon_{el}(0) k_B T / q^2 c_{Li}}$ is the Debye screening length and δ is the shift of the coordinates' origin from the metal surface (Figure 6). The parameter $\varepsilon_{el}(0)$ is the dielectric constant of the medium in which the concentration of free and localized lithium ions remains quite high. For LiPON with a lithium concentration of $c_{Li} \sim 10^{28}$ m^{-3}, the calculations give $\lambda_D = 1.2 \cdot 10^{-11}\sqrt{\varepsilon_{el}(0)}$ m. It is easy to verify that the solutions obtained satisfy the Poisson equation.

The EDL model makes it possible to calculate the capacitance of a double electrical layer as the capacitance of a parallel-plate capacitor, one of the plates of which is formed by potential-determining ions, and the other is an imaginary plane $x = L$ passing through the center of mass of the counterions (Figure 6b). The distance between these plates equals $L + \delta$, where $\delta = \ell + r_{Li}$, $\ell = 2.03$ Å is the bond length of $Li^+ - O^-$ [45], and $r_{Li} = 1.45 \cdot 10^{-10}$ m is the radius of the lithium atom.

The parameter L can be obtained from the following equation:

$$\int_0^L c_{O^-}(x)dx = \int_L^\infty c_{O^-}(x)dx \tag{15}$$

which gives $L = 0.69\lambda_D$ or $L = 8.3{\cdot}10^{-12}\sqrt{\varepsilon_{el}(0)}$. Considering (15), the expression for the EDL capacitance reduces to:

$$C_{EDL} = \frac{\varepsilon_0 \varepsilon_{el} S}{8.3{\cdot}10^{-12}\sqrt{\varepsilon_{el}} + \delta} \quad (16)$$

For $S = 4{\cdot}10^{-6}$ m^2 capacitance, (16) equals the fitting parameter $C_{EDL} = 9.70{\cdot}10^{-5}$ F at $\varepsilon_{el}(0) = 1.96{\cdot}10^3$. Finalizing the EDL topic, let us specify the value of the Debye shielding length, $\lambda_D = 5.31{\cdot}10^{-10}$ m; the center of mass coordinate, $L = 3.66{\cdot}10^{-10}$ m; and the distance between the plates of a parallel-plate capacitor simulating the EDL, $L + \delta = 7.14{\cdot}10^{-10}$ m.

The dielectric constant of LiPON in the depletion layer and in the bulk can vary significantly. The relation $A_A = d/S\varepsilon_0\varepsilon_{el}(0)$ allows us to determine the dielectric constant of LiPON, which, at $A_A = 1.31{\cdot}10^5\ \Omega{\cdot}s^{-1}$, proves to be $\varepsilon_{el} = 1.88{\cdot}10^4$. For fitting parameter $\rho = 3.5{\cdot}10^{-4}$, the appropriate value of the dielectric constant in the high-frequency limit is $\varepsilon_\infty = 6.6$.

Another feature of the proposed model is that the best approximation of the curves in Figure 4a is achieved at $\alpha = -0.015$. This signifies that the appropriate dissipative element in Cole and Cole model, known as a constant phase element, is a weak kinetic inductance. Since the mode of the mobile lithium ion oscillations is relaxation, the manifestation of kinetic inductance means a notable contribution of localized ion oscillations to the dielectric constant. It is also important that, at $\alpha < 0$ with $\omega \to 0$, the real part of absorption impedance tends to be zero: $ReZ_A \to 0$ as $\omega^{|\alpha|}$, while $ImZ_A \to -\infty$, i.e., the absorption element transforms into an ideal capacitor. At $\alpha > 0$, the real part, on the contrary, tends to infinity: $ReZ_A \to \infty$ as $1/\omega^\alpha$ with $\omega \to 0$. In both cases, the resistance of the absorption element tends to infinity, and the impedance of the diffusion element behaves similarly. Thus, in the limit $\omega \to 0$, the resistance of the circuit section $A \parallel R \parallel W_1$ in Figure 3 is determined only by ohmic losses and is equal to $R = \varepsilon(0)R_{int}$.

5. Summary

In conclusion, let us list the facts that testify in favor of the hypothesis regarding the absorption conductivity of LiPON and the existence of an electrical double layer. First of all, this is LiPON's high capacitance of dielectric absorption, also known as dielectric relaxation. Also, this is a large static dielectric constant value, an order of magnitude higher than the dielectric constant of ferroelectrics. Besides Bode diagrams, generated using an alternative equivalent circuit containing an absorbing element, we reproduced previously obtained experimental impedance spectra in detail. The hypothesis eliminates the obvious discrepancy between the high dielectric constant of LiPON and equivalent circuits, which in no way consider the effect of electric field shielding. The double electrical layer hypothesis allows us to relate the high apparent ohmic resistance to the fairly high intrinsic conductivity of LiPON, which also follows from the impedance of the absorption element. The apparent resistance value obtained from the fitting almost completely coincides with the product of the dielectric constant and the intrinsic resistance of LiPON. If the alternative LiPON impedance model is correct, then the conductivity results obtained in [28,31–38] should be attributed to dielectric losses.

Solid electrolytes are ionic conductors whose high dielectric constants are due to ionic relaxation polarization. To model the impedance of ionic conductors, constant phase elements are widely used. These elements, which have a physical meaning only for integer and half-integer values of the nonideality factor, make it possible to achieve a high degree of accuracy when approximating experimental curves. But at the same time, the fitting parameters of CPE do not carry any meaning and are of little use for understanding the mechanisms of polarization. The model of the absorption element and apparent active resistance proposed in the work expands the set of EIS structural elements, which makes it possible to abandon CPE when modeling ionic conductors.

A promising area of application for the obtained results may be the state of health estimation (SoH), an area that is becoming increasingly in demand as battery production develops. Accurate assessment of SoH is critical in order to optimize lithium-ion cell life and ensure safety during operation. In recent years, significant progress has been made in developing a methodology for monitoring lithium-ion cell degradation and estimating SoH based on electrochemical impedance spectroscopy measurements [46]. The LiPON equivalent circuit, modeling absorption, diffusion, drift, and leakage currents enable more accurate determination of SoH thresholds.

Author Contributions: A.R.—conceptualization, writing of original draft. A.N.—investigation. J.E.—investigation. All authors have read and agreed to the published version of the manuscript.

Funding: This research was funded by the Ministry of Science and Higher Education of the Russian Federation grant number FENZ-2024-0005.

Data Availability Statement: Data supporting the reported results can be obtained by demand from The Facilities Sharing Centre "Diagnostics of Micro- and Nanostructures" (FSC DMNS), P.G. Demidov Yaroslavl State University.

Conflicts of Interest: The authors declare that they have no conflicts of interest. The funders had no role in the design of the study; in the collection, analyses, or interpretation of data; in the writing of the manuscript, or in the decision to publish the results.

References

1. Tatsumisago, M. Glassy materials based on Li_2S for all-solid-state lithium secondary batteries. *Solid State Ion.* **2004**, *175*, 13–18. [CrossRef]
2. Mercier, R.; Malugani, J.-P.; Fahys, B.; Robert, G. Superionic conduction in $Li_2S-P_2S_5-LiI$—Glasses. *Solid State Ion.* **1981**, *5*, 663–666. [CrossRef]
3. Mizuno, F.; Hayashi, A.; Tadanaga, K.; Tatsumisago, M. New, highly ion-conductive crystals precipitated from $Li_2S-P_2S_5$ glasses. *Adv. Mater.* **2005**, *17*, 918–921. [CrossRef]
4. Hayashi, A.; Muramatsu, H.; Ohtomo, T.; Hama, S.; Tatsumisago, M. Improved chemical stability and cyclability in $Li_2S–P_2S_5–P_2O_5–ZnO$ composite electrolytes for all-solid-state rechargeable lithium batteries. *J. Alloys Compd.* **2014**, *591*, 247–250. [CrossRef]
5. Ohtomo, T.; Hayashi, A.; Tatsumisago, M.; Kawamoto, K. Characteristics of the $Li_2O–Li_2S–P_2S_5$ glasses synthesized by the two-step mechanical milling. *J. Non-Cryst. Solids* **2013**, *364*, 57–61. [CrossRef]
6. Trevey, J.E.; Gilsdorf, J.R.; Miller, S.W.; Lee, S.-H. $Li_2S–Li_2O–P_2S_5$ solid electrolyte for all-solid-state lithium batteries. *Solid State Ion.* **2012**, *214*, 25–30. [CrossRef]
7. Ujiie, S.; Hayashi, A.; Tatsumisago, M. Structure, ionic conductivity and electrochemical stability of $Li_2S–P_2S_5–LiI$ glass and glass–ceramic electrolytes. *Solid State Ion.* **2012**, *211*, 42–45. [CrossRef]
8. Ujiie, S.; Hayashi, A.; Tatsumisago, M. Preparation and ionic conductivity of $(100-x)$ $(0.8Li_2S·0.2P_2S_5)·xLiI$ glass–ceramic electrolytes. *J. Solid State Electrochem.* **2013**, *17*, 675–680. [CrossRef]
9. Zhang, Z.; Kennedy, J.H. Synthesis and characterization of the $B_2S_3-Li_2S$, the $P_2S_5-Li_2S$ and the $B_2S_3-P_2S_5-Li_2S$ glass systems. *Solid State Ion.* **1990**, *38*, 217–224. [CrossRef]
10. Stramare, S.; Thangadurai, V.; Weppner, W. Lithium lanthanum titanates: A review. *Chem. Mater.* **2003**, *15*, 3974–3990. [CrossRef]
11. Bohnke, O. The fast lithium-ion conducting oxides $Li_3xLa_{2/3-x}TiO_3$ from fundamentals to application. *Solid State Ion.* **2008**, *179*, 9–15. [CrossRef]
12. Inaguma, Y.; Liquan, C.; Itoh, M.; Nakamura, T.; Uchida, T.; Ikuta, H.; Wakihara, M. High ionic conductivity in lithium lanthanum titanate. *Solid State Commun.* **1993**, *86*, 689–693. [CrossRef]
13. Alonso, J.A.; Sanz, J.; Santamaría, J.; León, C.; Várez, A.; Fernández-Díaz, M.T. On the location of Li^+ cations in the fast Li-cation conductor $La_{0.5}Li_{0.5}TiO_3$ perovskite. *Angew. Chem. Int. Ed.* **2000**, *39*, 619–621. [CrossRef]
14. Ahn, J.-K.; Yoon, S.-G. Characteristics of amorphous lithium lanthanum titanate electrolyte thin films grown by PLD for use in rechargeable lithium microbatteries. *Electrochem. Solid-State Lett.* **2005**, *8*, A75–A78. [CrossRef]
15. Hagman, L.O.; Kierkegaard, P.; Karvonen, P.; Virtanen, A.I.; Paasivirta, J. The crystal structure of $NaMe_2$ IV $(PO_4)_3$; MeIV = Ge, Ti, Zr. *Acta Chem. Scand.* **1968**, *22*, 1822–1832. [CrossRef]
16. Hong, H.P. Crystal structures and crystal chemistry in the system $Na_{1+x}Zr_2Si_xP_{3-x}O_{12}$. *Mater. Res. Bull.* **1976**, *11*, 173–182. [CrossRef]
17. Kosava, N.V.; Devyatkina, E.T.; Stepanov, A.P.; Buzlukov, A.L. Lithium conductivity and lithium diffusion in NASICON-type $Li_{1+x}Ti_{2-x}Al_x(PO_4)_3$ (x= 0; 0.3) prepared by mechanical activation. *Ionics* **2008**, *14*, 303–311. [CrossRef]
18. Goodenough, J.B.; Hong, H.Y.-P.; Kafalas, J.A. Fast Na^+-ion transport in skeleton structures. *Mater. Res. Bull.* **1976**, *11*, 203–220. [CrossRef]

19. Hong, H.-P. Crystal structure and ionic conductivity of $Li_{14}Zn(GeO_4)_4$ and other new Li^+ superionic conductors. *Mater. Res. Bull.* **1978**, *13*, 117–124. [CrossRef]
20. Kamaya, N.; Homma, K.; Yamakawa, Y.; Hirayama, M.; Kanno, R.; Yonemura, M.; Kamiyama, T.; Kato, Y.; Hama, S.; Kawamoto, K.; et al. A lithium superionic conductor. *Nat. Mater.* **2011**, *10*, 682–686. [CrossRef]
21. Takada, K.; Inada, T.; Kajiyama, A.; Sasaki, H.; Kondo, S.; Watanabe, M.; Murayama, M.; Kanno, R. Solid-state lithium battery with graphite anode. *Solid State Ion.* **2003**, *158*, 269–274. [CrossRef]
22. Inada, T.; Kobayashi, T.; Sonoyama, N.; Yamada, A.; Kondo, S.; Nagao, M.; Kanno, R. All solid-state sheet battery using lithium inorganic solid electrolyte, thio-LISICON. *J. Power Sources* **2009**, *194*, 1085–1088. [CrossRef]
23. Yu, C.-E.; Gregory, D.H.; Liu, W.-R. $Li_{1.3}Al_{0.3}Ti_{1.7}(PO_4)_3$ (LATP) solid electrolytes synthesized by microwave-assisted hydrothermal reactions for Li all-solid-state battery applications. *Surf. Coat. Technol.* **2024**, *481*, 130671. [CrossRef]
24. Bates, J.B.; Dudney, N.J.; Gruzalski, G.R.; Zuhr, R.A.; Choudhury, A.; Luck, C.F.; Robertson, J.D. Electrical properties of amorphous lithium electrolyte thin films. *Solid State Ion.* **1992**, *53–56*, 647–654. [CrossRef]
25. Bates, J.B.; Dudney, N.J.; Gruzalski, G.R.; Zuhr, R.A.; Choudhury, A.; Luck, C.F.; Robertson, J.D. Fabrication and characterization of amorphous lithium electrolyte thin films and rechargeable thin-film batteries. *J. Power Sources* **1993**, *43*, 103–110. [CrossRef]
26. Bates, J.B.; Gruzalski, G.R.; Dudney, N.J.; Luck, C.F.; Yu, X. Rechargeable thin-film lithium batteries. *Solid State Ion.* **1994**, *619*, 70–71. [CrossRef]
27. Bates, J.B.; Dudney, N.J.; Lubben, D.C.; Gruzalski, G.R.; Kwak, B.S.; Yu, X.; Zuhr, R.A. Thin-film rechargeable lithium batteries. *Ibid* **1995**, *58*, 54. [CrossRef]
28. Yu, X.; Bates, J.B.; Jellison, G.E., Jr.; Hart, F.X. A Stable Thin-Film Lithium Electrolyte: Lithium Phosphorus Oxynitride. *J. Electrochem. Soc.* **1997**, *144*, 524–532. [CrossRef]
29. Yu, X.; Bates, J.B.; Jellison, G.E. Proceedings of the Symposium on Thin Film Solid Ionic Devices and Materials. *Electrochem. Soc.* **1995**, *95*, 23.
30. Bates, J.B.; Dudney, N.J.; Luck, C.F.; Sales, B.C.; Zuhr, R.A. Deposition and characterization of Li_2O–SiO_2–P_2O_5 thin films. *J. Am. Ceram. Soc.* **1993**, *76*, 929–943. [CrossRef]
31. Hamon, Y.; Douard, A.; Sabary, F.; Marcel, C.; Vinatier, P.; Pecquenard, B. Influence of sputtering conditions on ionic conductivity of LiPON thin films. *Solid State Ion.* **2006**, *177*, 257–261. [CrossRef]
32. Li, L.; Liu, S.; Xue, X.; Zhou, H. Effects of rough interface on impedance of solid LiPON in MIM cells. *Ionics* **2018**, *24*, 351–362. [CrossRef]
33. Mascaraque, N.; Fierro, J.L.G.; Durán, A.; Muñoz, F. An interpretation for the increase of ionic conductivity by nitrogen incorporation in LiPON oxynitride glasses. *Solid State Ion.* **2013**, *233*, 73–79. [CrossRef]
34. Nimisha, C.S.; Rao, G.M.; Munichandraiah, N.; Natarajan, G.; Cameron, D.C. Chemical and microstructural modifications in LiPON thin films exposed to atmospheric humidity. *Solid State Ion.* **2011**, *185*, 47–51. [CrossRef]
35. Le Van-Jodin, L.; Ducroquet, F.; Sabary, F.; Chevalier, I. Dielectric properties, conductivity and Li+ ion motion in LiPON thin films. *Solid State Ion.* **2013**, *253*, 151–156. [CrossRef]
36. Muñoz, F.; Dur'an, A.; Pascual, L.; Montagne, L.; Revel, B.; Rodrigues, A.C.M. Increased electrical conductivity of LiPON glasses produced by ammonolysis. *Solid State Ion.* **2008**, *179*, 574–579. [CrossRef]
37. Fleutot, B.; Pecquenard, B.; Martinez, H.; Levasseur, A. Thorough study of the local structure of LiPON thin films to better understand the influence of a solder-reflow type thermal treatment on their performances. *Solid State Ion.* **2012**, *206*, 72–77. [CrossRef]
38. Su, Y.; Falgenhauer, J.; Polity, A.; Leichtweiß, T.; Kronenberger, A.; Obel, J.; Zhou, S.; Schlettwein, D.; Janek, J.; Meyer, B.K. LiPON thin films with high nitrogen content for application in lithium batteries and electrochromic devices prepared by RF magnetron sputtering. *Solid State Ion.* **2015**, *282*, 63–69. [CrossRef]
39. L'opez-Grande, A.; Mather, G.C.; Muñoz, F. Thermodynamic calculation of the ionic conductivity of LiPON glasses and solid electrolytes†. *J. Mater. Chem. A* **2023**, *11*, 12282. [CrossRef]
40. Rudyi, A.S.; Lebedev, M.E.; Mironenko, A.A.; Mazaletskii, L.A.; Naumov, V.V.; Novozhilova, A.V.; Fedorov, I.S.; Churilov, A.B. Study of the relaxational rolarization dynamics of the LiPON solid electrolyte. *Russ. Microelectron.* **2020**, *49*, 345. [CrossRef]
41. Krohns, S.; Lunkenheimer, P.; Kant, C.; Pronin, A.V.; Brom, H.B.; Nugroho, A.A.; Loidl, A. Colossal dielectric constant up to GHz at room temperature. *Appl. Phys. Lett.* **2009**, *94*, 122903. [CrossRef]
42. Kenneth, S.; Robert, H. Cole Dispersion and Absorption in Dielectricsıo 1. Alternating Current Characteristics. *J. Chem. Phys.* **1941**, *9*, 341–351.
43. Rudy, A.; Mironenko, A.; Naumov, V.; Novozhilova, A.; Skundin, A.; Fedorov, I. Determination of Diffusion Coefficients of Lithium in Solid Electrolyte LiPON. *Batteries* **2021**, *7*, 21. [CrossRef]
44. Vasilev, S.V.; Lebedev, M.E.; Mazaletskii, L.A.; Metlitskaya, A.V.; Mironenko, A.A.; Naumov, V.V.; Novozhilova, A.V.; Rudyi, A.S.; Fedorov, I.S. Development of the technology of magnetron sputtering deposition of LiPON films and investigation of their characteristics. *Russ. Microelectron.* **2017**, *46*, 424–432. [CrossRef]

45. Lacivita, V.; Westover, A.S.; Kercher, A.K.; Phillip, N.D.; Yang, G.; Veith, G.M.; Ceder, G.; Dudney, N.J. Resolving the Amorphous Structure of Lithium Phosphorus Oxynitride (Lipon). *J. Am. Chem. Soc.* **2018**, *140*, 11029–11038. [CrossRef]
46. Iurilli, P.; Brivio, C.; Carrillo, R.E.; Wood, V. Physics-Based SoH Estimation for Li-Ion Cells. *Batteries* **2022**, *8*, 204. [CrossRef]